UHASSELT
KNOWLEDGE IN ACTION

Maastricht University

Faculty of Medicine and Life Sciences
School for Life Sciences
Master of Biomedical Sciences

Master's thesis

MiR146A as novel target to mitigate phagocytic lipid overload in multiple sclerosis

Dylan Kidjemet

Thesis presented in fulfillment of the requirements for the degree of Master of Biomedical Sciences, specialization Molecular Mechanisms in Health and Disease

SUPERVISOR :

Prof. dr. Jeroen BOGIE

MENTOR :

De heer Sam VANHERLE

2023
2024

Transnational University Limburg is a unique collaboration of two universities in two countries: the University of Hasselt and Maastricht University.

UHASSELT
KNOWLEDGE IN ACTION

www.uhasselt.be
Universiteit Hasselt
Campus Hasselt:
Martelarenlaan 42 | 3500 Hasselt
Campus Diepenbeek:
Agoralaan Gebouw D | 3590 Diepenbeek

Faculty of Medicine and Life Sciences
School for Life Sciences
Master of Biomedical Sciences

Master's thesis

MiR146A as novel target to mitigate phagocytic lipid overload in multiple sclerosis

Dylan Kidjemet

Thesis presented in fulfillment of the requirements for the degree of Master of Biomedical Sciences, specialization Molecular Mechanisms in Health and Disease

SUPERVISOR :

Prof. dr. Jeroen BOGIE

MENTOR :

De heer Sam VANHERLE

MiR-146A as novel target to mitigate phagocytic lipid overload in multiple sclerosis*

Dylan Kidjemet[1], Sam Vanherle[1], Jeroen Bogie[1]

[1]Morphology research group, Biomedical Research Institute, Universiteit Hasselt, Campus Diepenbeek,
Agoralaan Gebouw C - B-3590 Diepenbeek

*Running title: *miR-146A to mitigate lipid overload in MS*
To whom correspondence should be addressed: Jeroen Bogie; Email: jeroen.bogie@uhasselt.be

Keywords: multiple sclerosis, myelin-containing phagocytes, lipid metabolism, miR-146A

ABSTRACT

Phagocytes play an essential role in lipid metabolism within the central nervous system (CNS) and have been implicated in various diseases, including multiple sclerosis (MS). Recent studies have highlighted the link between defective myelin debris clearance by phagocytes and the lack of remyelination observed in progressive MS patients. The efficient clearance of myelin debris by phagocytes, such as macrophages and microglia, is crucial for remyelination and preventing neurodegeneration. However, in MS, this process is often impaired, leading to the accumulation of myelin debris and subsequent chronic inflammation. MicroRNAs (miRNAs) are key players in negatively regulating various biological processes, including lipid metabolism. Understanding the function of miRNAs in the context of lipid droplet metabolism and inflammation in MS could provide valuable insights into potential therapeutic targets.

Here, we identify miR-146A, previously associated with atherosclerosis and other inflammatory conditions, as an important regulator of lipid droplet processing. This study focuses on elucidating the impact of miR-146A on lipid metabolism and phagocytic function in macrophages, potentially offering therapeutic avenues for progressive MS and related demyelinating disorders.

INTRODUCTION

Multiple sclerosis (MS) is an autoimmune-mediated disease of the central nervous system (CNS) that leads to demyelination, the destruction of the protective layer around axons. Insufficient remyelination, the formation of new myelin sheets, causes neurons to degenerate and partly explains the lack of regeneration seen in MS patients. Although current therapies for MS postpone symptoms, no curative treatment exists for patients with a progressive disease form. Intriguingly, our research group and others have highlighted a link between the lack of remyelination in progressive MS and malfunctioning phagocytes (1,2).

Phagocytes, such as macrophages and CNS-resident microglia, are key players in the pathogenesis of MS (3). Their ability to rapidly respond to changes in the microenvironment, such as the release of myelin debris, allows polarization between disease-promoting M1 and disease-resolving M2 phenotype (1,4). The latter is essential for efficient remyelination as it drives the differentiation of oligodendrocyte precursor cells into myelin-forming oligodendrocytes by releasing trophic factors, promoting myelin debris clearance, and resolving inflammation (5,6). Although a pro-regenerative, anti-inflammatory M2 phenotype can be observed in response to the clearance of myelin debris and trophic factor release, this is only temporary (1,4). Sustained myelin internalization polarizes phagocytes towards a proinflammatory M1 phenotype that suppresses remyelination, as excessive amounts of myelin-derived lipids overwhelm the efflux capacity of phagocytes (1,2). Accordingly, data from our research group show an increased intracellular cholesterol load within phagocytes in response to myelin-derived lipid overload, leading to a disease-promoting phagocytic phenotype (1,2). This highlights the importance of pharmacologically targeting lipid metabolism within phagocytes to mitigate inflammation and potentially enhance remyelination in MS.

MicroRNAs (miRNAs) are non-coding RNAs that post-transcriptionally regulate diverse

biological processes, including lipid metabolism (7,8), by binding to target messenger RNAs (mRNAs), leading to mRNA degradation or translational repression (9). Emerging evidence indicates that dysregulation of miRNAs leads to autoimmunity and neurodegeneration (10) and has therefore been implicated in various diseases, including MS (11). However, the intricate interplay between dysregulated lipid metabolism in phagocytes and miRNAs remains to be elucidated in the context of MS. We hypothesize that targeting miRNAs could relieve lipid overload and improve phagocytic function. Understanding how miRNAs regulate lipid metabolism and inflammation and their subsequent downstream effects on remyelination and neurodegeneration could unveil a therapeutic avenue for progressive MS patients and others with demyelinating pathologies.

Here, we report that miR-146A exacerbates phagocytic lipid droplet accumulation and inflammation upon myelin exposure. We demonstrate that transfection of miR-146A inhibitor mitigates lipid overload and reduces inflammation, thereby preventing the myelin overload-induced phenotypic shift. Our findings highlight the importance of miRNAs in controlling phagocytic lipid metabolism in MS.

EXPERIMENTAL PROCEDURES

Mice – Wild-type C57BL/6J mice were purchased from Envigo. Mice were housed on a 12h light/dark circadian rhythm with *ad libitum* access to water and a standard chow diet. All procedures were conducted in accordance with the institutional guidelines and were approved by the Ethical Committee for Animal Experiments of Hasselt University.

Myelin isolation – Murine myelin was purified in-house from postmortem mouse brain tissue of 10-week-old male and female C57BL6/J mice using density gradient centrifugation, as previously performed (12). In short, brain tissue was homogenized in 0.32M sucrose and layered on top of 0.85M sucrose. Next, the myelin was isolated by means of centrifugation at 75,000g before being washed and purified in water.

Cell isolation and culture – Bone marrow-derived macrophages (BMDMs) were isolated as previously performed (12). Bone marrow cells from the tibia and femur were harvested from 11-week-old female WT mice by inserting a needle into the bone and flushing with 1x PBS. These were then cultured in 14.5 cm Petri dishes (Greiner) at a concentration of 10×10^6 cells/dish using RMPI-1640 medium supplemented with 10% fetal calf serum (FCS; Biowest), 50U/mL penicillin (Invitrogen), 50U/mL streptomycin (Invitrogen), and 15% L929-conditioned medium (LCM) for 7 days. Afterward, the cells were cultured at a density of 0.5×10^6 cells/mL in RPMI-1640 medium (Gibco) supplemented with 10% FCS, 50 U/mL penicillin, 50 U/mL streptomycin, and 5% LCM. These were then treated daily with 100µg/mL murine myelin for 24h or 72h before analysis.

RNA isolation / cDNA Synthesis / qPCR – Cells were lysed using Qiazol lysis reagent (Qiagen). Total RNA was extracted using the RNeasy mini kit (Qiagen) according to the manufacturer's instructions. To assess miRNA expression, the miRNeasy Micro Kit (Qiagen) was used according to the manufacturer's protocol. Precipitated RNA was dissolved in nuclease-free water. Concentration and purity were measured using NanoDrop™ 2000 (Thermo Scientific) by measuring the absorbance ratio at 260 and 280 nm. cDNA was synthesized using either the qScript cDNA synthesis kit (Quanta Biosciences) for RNA or the miRCURY™ LNA RT kit (Qiagen) for miRNA, according to the manufacturer's instructions. The cDNA was then amplified and detected using the miRCURY™ LNA SYBR® Green PCR kit (Qiagen) with the use of the T100™ thermal cycler (Bio-Rad Laboratories) under the following conditions: 25°C for 5 min, 42°C for 30 min, 85°C for 5 min for cDNA synthesis from RNA or 42°C for 60 min, 95°C for 5 min for first-strand cDNA synthesis from miRNA. The expression of genes was assessed using the Quantstudio™ 3 detection system (Applied Biosystems). Results were normalized to the expression of the most stable reference genes as determined by GeNorm, being *Tbp* and *Cyca* for mRNA or *U6* and *Rnu5g* for miRNA, and were quantified by the comparative Ct method. Primer sequences are listed in supplementary Table **S1**.

RNA sequencing – Tissue or cells were lysed using QIAzol. RNA was extracted using the RNeasy mini kit (Qiagen). Total RNA content was analyzed with a Nanodrop 1000 spectrophotometer (Thermo Fisher Scientific). RNA samples were processed by the Genomics

Core Leuven (Belgium). The R-based Bioconductor package DESeq2 (The R Foundation for Statistical Computing) was used for count-based differential expression analysis of a single gene. Differentially expressed genes were identified based on a log2-fold change <−0.5 and >0.5 and a P-value < 0.05.

Transfection – BMDMs were transfected using Lipofectamine RNAiMAX™ reagent (Invitrogen) according to the manufacturer's instructions. Briefly, after 24h of seeding BMDMs, 1µL of Lipofectamine reagent and miRNA mimic, antagomir, or scramble were diluted separately in 25µL of reduced serum Opti-MEM® I medium (Gibco) and allowed to incubate for 5 min. Next, the diluted miRNA was combined with the Lipofectamine reagent in a 1:1 ratio. The transfection lipid complex was incubated at RT for 20 min before adding 2.5 nM (mimic/scramble) or 100 nM (antagomir/scramble) to each well. Cells were incubated with the transfection lipid complex for 48h at 37 °C with 5% CO_2, after which the medium was replaced with reduced-serum Opti-MEM® I medium and the cells were treated daily with 100 µg/mL of myelin for either 24h or 72h and collected for downstream analysis. The miRNAs used include miRCURY™ LNA miR-146A Power Inhibitor (Qiagen), Mimic (Qiagen), and Negative Control (Qiagen).

Flow cytometry – Intracellular lipid load in BMDMs was assessed by incubating the cells with BODIPY (493/503, 2 µM, Invitrogen) for 15 min at 37 °C and protected from light. Cellular fluorescence was quantified using the LSRFortessa™ (BD Biosciences). Data is represented as relative lipid load compared to vehicle.

Phagocytosis assay – To assess the ability of BMDMs to phagocytose myelin, myelin was fluorescently labeled with 1,1'-dioctadecyl-3,3,3',3'-tetramethylindocarbocyanine perchlorate (DiI, Sigma-Aldrich) or PhRodo (Thermo Fisher). After treating the BMDMs with 100 µg/mL DiI or PhRodo myelin for 1.5h at 37 °C and protected from light, the BMDMs were analyzed for fluorescence intensity by using the LSRFortessa™ (BD Biosciences) or CLARIOstar® Plus Microplate Reader (BMG Labtech), respectively. Data is represented as relative uptake compared to vehicle.

Cholesterol efflux assay – Total cholesterol (TC) was measured in BMDM lysates using the Amplex™ Red Cholesterol Assay (Thermo Fisher Scientific), according to the manufacturer's instructions. To define cholesterol efflux, BMDMs were exposed to ApoA-I (50 µg/mL) in phenol- and serum-free medium for 4h at 37°C before measuring intracellular and extracellular TC. Cholesterol efflux was determined by dividing fluorescence in the supernatants by the total fluorescence in the supernatants and cells. Fluorescence was measured by excitation wavelength of 540 nm and emission of 590 nm wavelength using a CLARIOstar® Plus Microplate Reader (BMG Labtech).

ORO staining – To visualize esterified cholesterol, cells were fixed with 4% paraformaldehyde followed by incubation in 0.3 % Oil Red O (ORO, Sigma-Aldrich) for 10 min, while cell nuclei were counterstained using hematoxylin (Merck) for 1 min at RT. Representative images were taken using a Leica DM 2000 LED microscope at 40x magnification. Analysis was performed with Fiji ImageJ software using an in-house script. Data is represented as ORO positive area per cell compared to vehicle. For quantitative measurements, the staining was eluted with 100% isopropanol (Fisher Chemical). These quantitative ORO analyses were performed by measuring the absorbance at 510 nm using a CLARIOstar® Plus Microplate Reader (BMG Labtech).

Statistical analysis – Data were reported as mean ± s.e.m. and statistically analyzed using GraphPad Prism 10. To test whether the data was normally distributed a D'Agostino-Pearson omnibus test was used. Normally distributed datasets were analyzed using a one-way ANOVA or two-tailed unpaired Student's *t*-test to test for comparisons between groups. P values < 0.05 were considered statistically significant. (*, P < 0.05; **, P < 0.01; ***, P < 0.001; ****, P < 0.0001).

RESULTS

miR-146A expression levels significantly altered in MS lesions and phagocytes – MicroRNAs (miRNAs) play critical roles in the regulation of gene expression, influencing various cellular processes, including inflammation and lipid metabolism (9,13). In the context of MS, macrophages and microglia are key players in

myelin degradation and inflammation, making them potential targets for studying miRNA functions (3).

Accordingly, samples are taken from human active MS lesions and surrounding normal-appearing white matter (NAWM), for subsequent miRNA expression analysis. In addition, miRNA expression levels are analyzed in myelin-treated macrophages and microglia and compared to untreated macrophages and microglia (control). Among the hundreds of miRNAs tested, we identified the 30 most significant miRNA hits based on the highest p-value. To facilitate the identification of miRNA expression patterns, the expression levels are arranged in a heat map (Figure **1A**, **1B**).

Furthermore, to identify common miRNA hits across the three datasets, we performed a Venn diagram analysis, showing miR-146A and miR155 being upregulated in myelin-treated macrophages, myelin-treated microglia, and active MS lesions compared to their respective control. (Figure **1C**). Collectively, these findings highlight miR-146A and miR-155 as potential key players implicated in MS pathogenesis. In this study, miR-146A is chosen for detailed analysis.

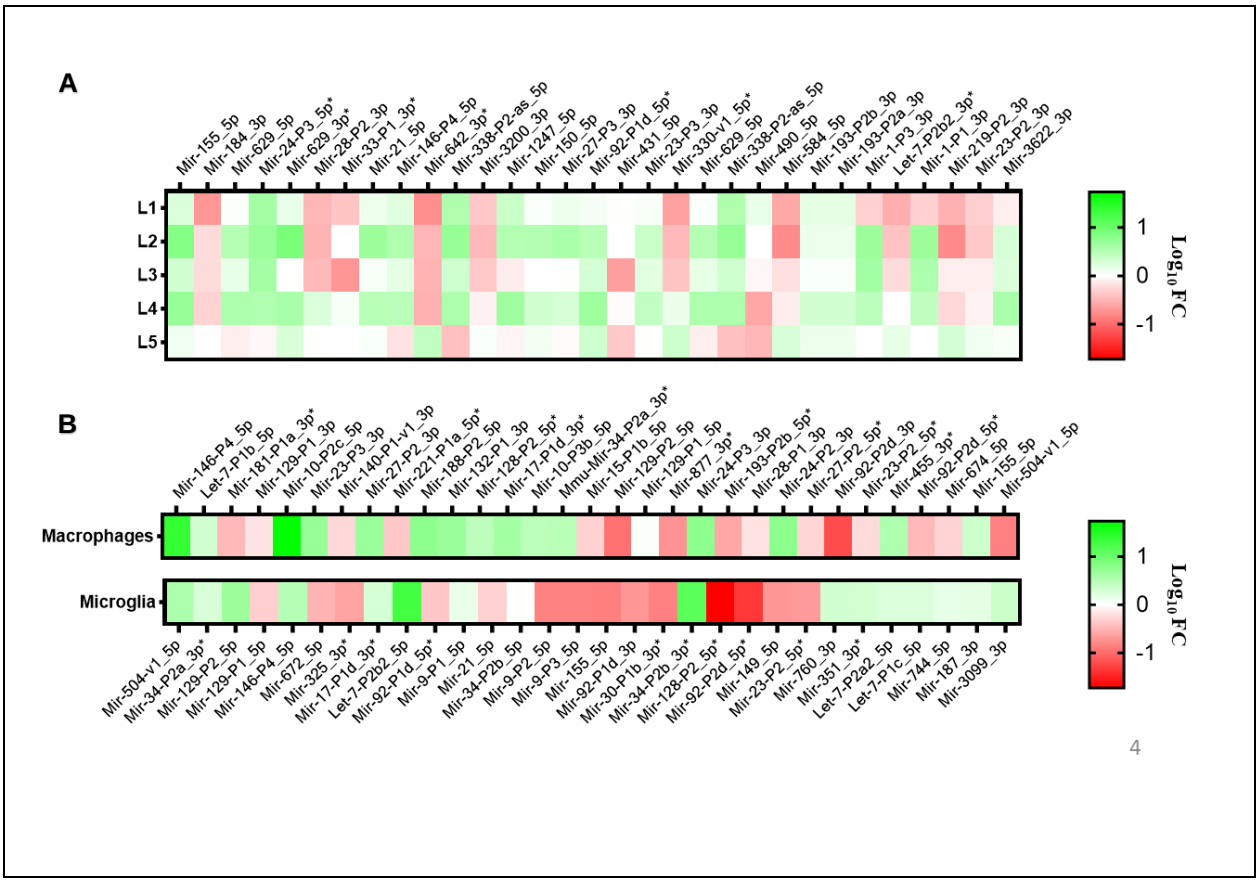

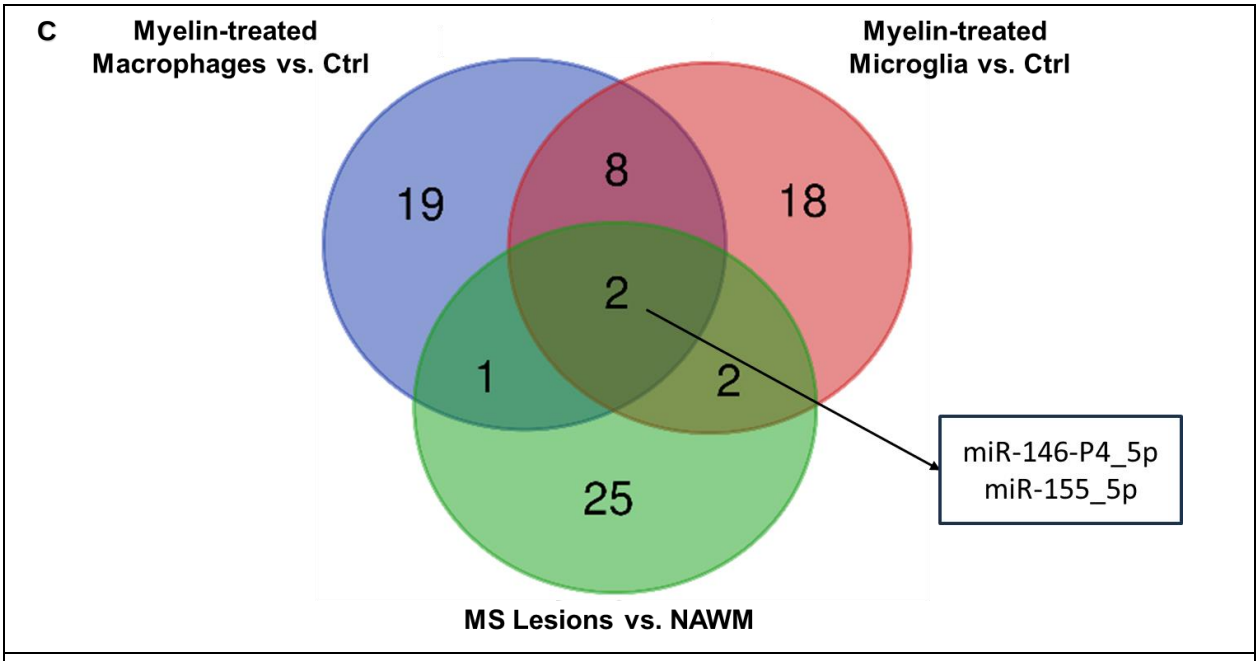

Fig. 1: miR-146A expression levels significantly altered in MS lesions and phagocytes – (**A**) Heat map analysis of the 30 most significant differences in miRNA expression levels, as determined by the highest p-value, in Multiple Sclerosis (MS) lesions (*n* = 5, L1-L5) compared to normal-appearing white matter (NAWM), (**B**) and myelin-treated macrophages (*n* = 5), and microglia (*n* = 5), compared to their respective untreated control. Data are indicated as log10 fold change (Log_{10} FC) of miRNA expression. (**C**) Venn diagram showing overlapping miRNA hits common to all three datasets; [myelin-treated macrophages vs. Ctrl (blue); myelin-treated microglia vs. Ctrl (red); MS lesions vs. NAWM (green)]. *Ctrl = control*.

Transfection with mimic or antagomir alters expression of miR-146A – To investigate the impact of miR-146A on *in vitro* lipid metabolism and inflammation, wild-type (WT) bone marrow-derived macrophages (BMDMs) were transfected with miR-146A mimic (2.5 nM), inhibitor (antagomir, 100 nM), or negative control (scramble). To evaluate if sustained myelin accumulation influences transfection efficiency, BMDMs were incubated with myelin for a short duration, prolonged, or left untreated (Figure **2A**). Accordingly, mimics and antagomir successfully up-, and downregulate miR-146A expression, respectively, in both untreated and short-term myelin-exposed BMDMs. Notably, after 72 hours, the effects of miR-146A mimic or antagomir transfection begin to diminish, and the expression levels of miR-146A return to physiological levels upon prolonged myelin exposure. Consistent with these findings, transfection efficiency is confirmed by quantitative PCR, as evidenced by the significant overexpression and knockdown of miR-146A in mimic- and antagomir-treated BMDMs, respectively (Figure **2B**).

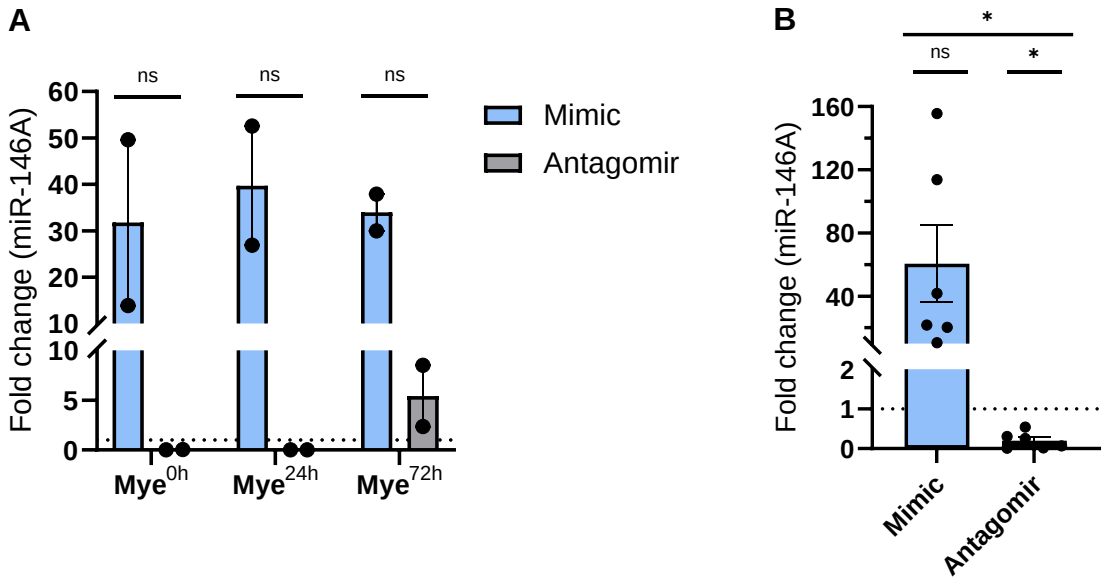

Fig. 2: Transfection with mimic or antagomir alters expression of miR-146A – (**A**) miR-146A expression levels in wild-type (WT), myelin-treated (100 µg/mL, 0h, 24h or 72h) bone marrow-derived macrophages (BMDMs) (*n* = 2 wells) transfected with miR-146A mimic (2.5 nM), inhibitor (antagomir, 100 nM), or negative control (scramble). (**B**) miR-146A expression levels in BMDMs (*n* = 6 wells) transfected with miR-146A mimic, antagomir or scramble. Data is represented as mean ± SEM. (*, P < 0.05). The dotted lines represent myelin-treated cells exposed to scramble.

Targeting miR-146A mitigates myelin debris overload – Considering that impaired lipid processing and the resulting accumulation of myelin-derived cholesterol and lipid droplets in macrophages and microglia contribute to phenotypic switch from disease-resolving macrophages into the disease-promoting phenotype in demyelinating pathologies (1,2,14), we next aimed to determine the effect of miR-146A modulation on lipid metabolism *in vitro*. We observed a decreased and, albeit not significant, increased cellular lipid formation in BMDMs upon transfection with miR-146A antagomir and mimic, respectively, as evidenced by a decreased cellular oil red O (ORO) load (Figure **3A, B**).

Since previous research has demonstrated that long-term exposure to myelin makes BMDMs more foamy compared to short-term exposure (15), we aimed to determine the impact of miR-146A on lipid load after prolonged myelin exposure. As anticipated, transfection of BMDMs with miR-146A mimics significantly increased the cellular ORO load upon prolonged myelin exposure (Figure **3C**). Yet, despite the increased lipid load upon transfection with miR-146A mimic, we found no decrease in ORO load in antagomir-treated BMDMs. On the contrary, the knockdown of miR-146A with antagomir significantly decreased the lipid load, and to a greater extent upon prolonged myelin exposure, as confirmed by the decreased BODIPY fluorescence intensity in the antagomir-treated BMDMs (Figure **3D**). Regardless, the effects of prolonged myelin exposure upon transfection with miR-146A mimics are not pronounced in the fluorescence intensity of BODIPY.

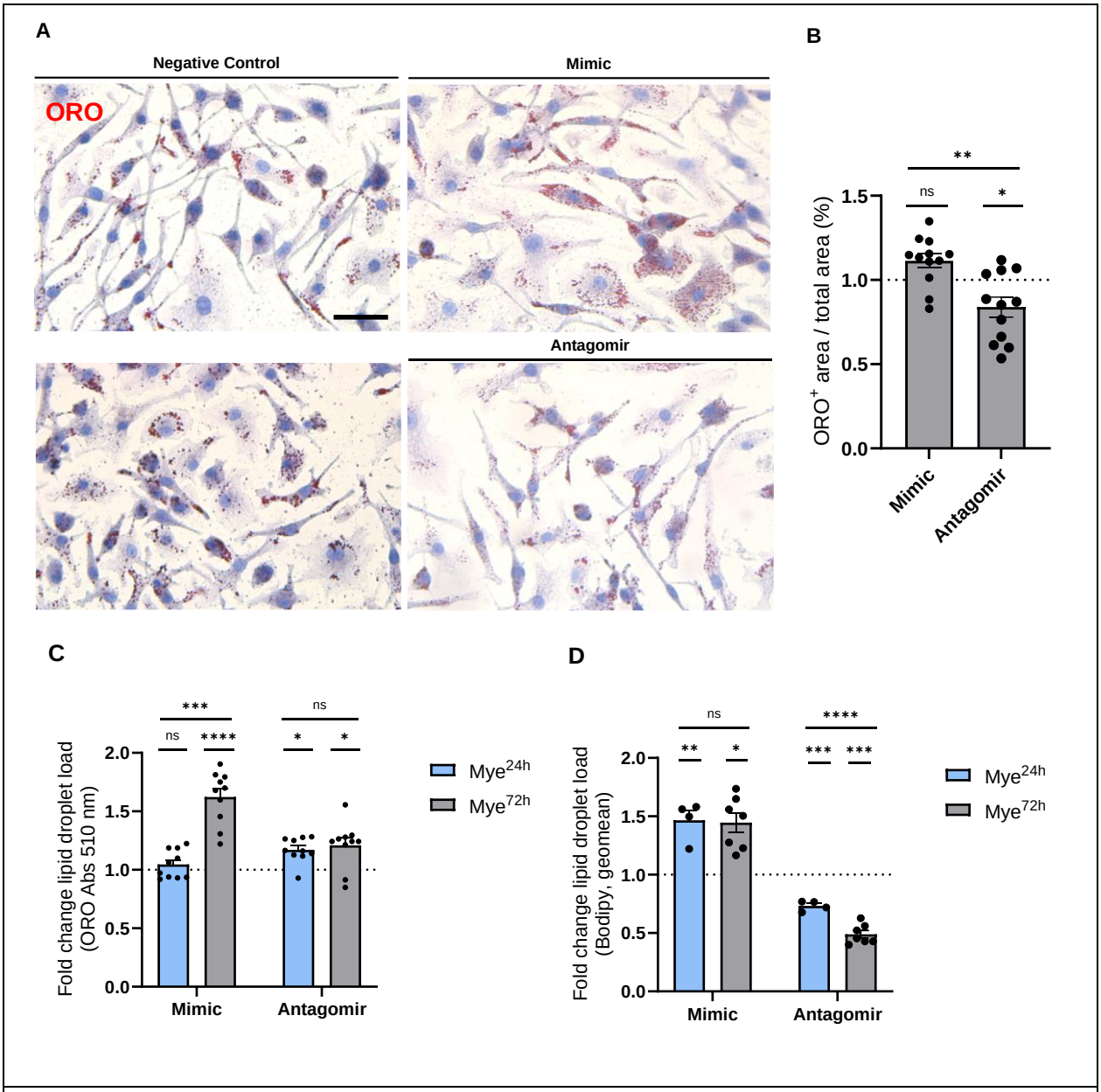

Fig. 3: Targeting miR-146A mitigates myelin debris overload – (**A, B**) Representative images and quantification (% cell area covered with lipid droplets) of an oil red O (ORO) staining on myelin-treated (100 µg/mL, 72h) BMDMs (*n* = 5 wells) transfected with miR-146A mimic (2.5 nM), antagomir (100 nM), or scramble. Scale bar, 20 µm. (**C**) Quantification of ORO-stained lipid droplets in myelin-treated (24h or 72h) WT BMDMs (*n* = 10 wells) transfected with miR-146A mimic, antagomir or scramble by measuring absorbance at 510 nm. (**D**) Mean fluorescence intensity of BODIPY in myelin-treated (100 µg/mL, 24h or 72h) BMDMs (24h; *n* = 4 wells, 72h; *n* = 7 wells) exposed to either mimic, antagomir, or scramble. Data is represented as mean ± SEM. (*, P < 0.05; **, P < 0.01; ***, P < 0.001; ****, P < 0.0001). The dotted lines represent myelin-treated cells exposed to scramble.

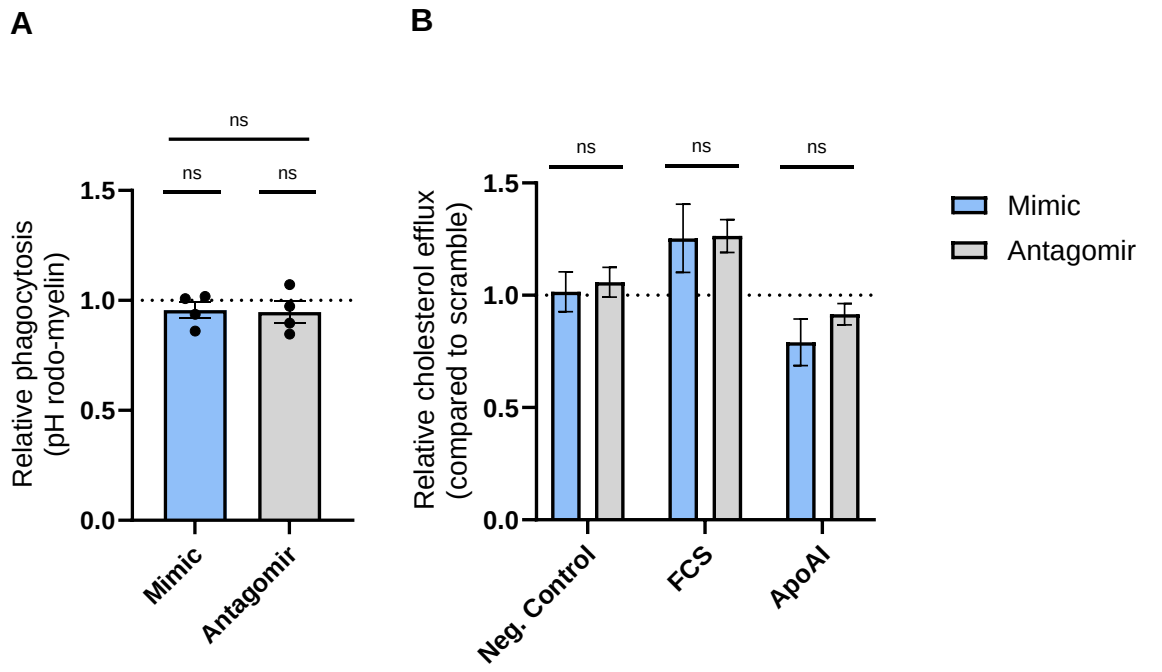

Fig. 4: Lipid uptake and efflux are not affected by miR-146A modulation – (**A**) Internalization of PhRodo-labeled myelin (100 µg/mL, 1.5h) by WT BMDMs (*n* = 4 wells) exposed to miR-146A mimic, antagomir, or vehicle. (**B**) Relative capacity to efflux total cholesterol (TC) of myelin-treated (72h) WT BMDMs (*n* = 5 wells) exposed to either miR-146A mimic, antagomir, or scramble. Data is represented as mean ± SEM. The dotted lines represent myelin-treated cells exposed to scramble.

Lipid uptake and efflux are not affected by miR-146A modulation – So far, we have established that transfection with miR-146A mimics increases lipid droplet load in BMDMs. Given that the cellular lipid droplet pool and composition are regulated by changes in lipid uptake, synthesis, and efflux (16,17), we next aimed to define the effect of miR-146A on the phagocytotic capacity of macrophages (Figure **4A**). Phagocytosis experiments revealed no significant differences in fluorescently labeled myelin uptake by BMDMs transfected with mimic or antagomir. Subsequently, we investigated the degree of total cholesterol (TC) efflux (Figure **4B**), considering the lack of effect on lipid uptake. Interestingly, the increased lipid load upon transfection with miR-146A mimics is not accompanied by an increased uptake, nor by a decrease in efflux.

Altogether, these results suggest that another mechanism, such as enhanced *de novo* synthesis of lipid droplets, may be contributing to the observed lipid accumulation in miR-146A mimic-treated BMDMs.

MiR146A overexpression skews macrophages towards an inflammatory phenotype – Given that increased lipid load is associated with inflammation (1,18), and that miR-146A modulation is indicated in attenuating inflammation in *in vitro* and *in vivo* models of atherosclerosis (19,20), we next investigated whether miR-146A overexpression could polarize macrophages towards an anti-inflammatory phenotype. Counterintuitively, we found an increased expression of inflammatory mediators, especially chemokine ligands *Ccl4* and *Ccl5*, in the miR-146A mimic-treated BMDMs compared to antagomir-treated under LPS-, and IFNg-stimulation (Figure **5A**). In addition, we examined the expression of genes involved in lipid metabolism to gain a comprehensive understanding of how miR-146A modulation affects lipid droplet metabolism (Figure **5B**). To our surprise, miR-146A antagomir significantly increased expression levels of *Acc2*, a rate-

limiting enzyme in the *de novo* synthesis of fatty acids (21), and *Fasn*, another key enzyme in the lipogenesis pathway (22). In contrast, inhibition of miR-146A also up-regulated the expression of *Pparα*, a key regulator of fatty acid oxidation (23).

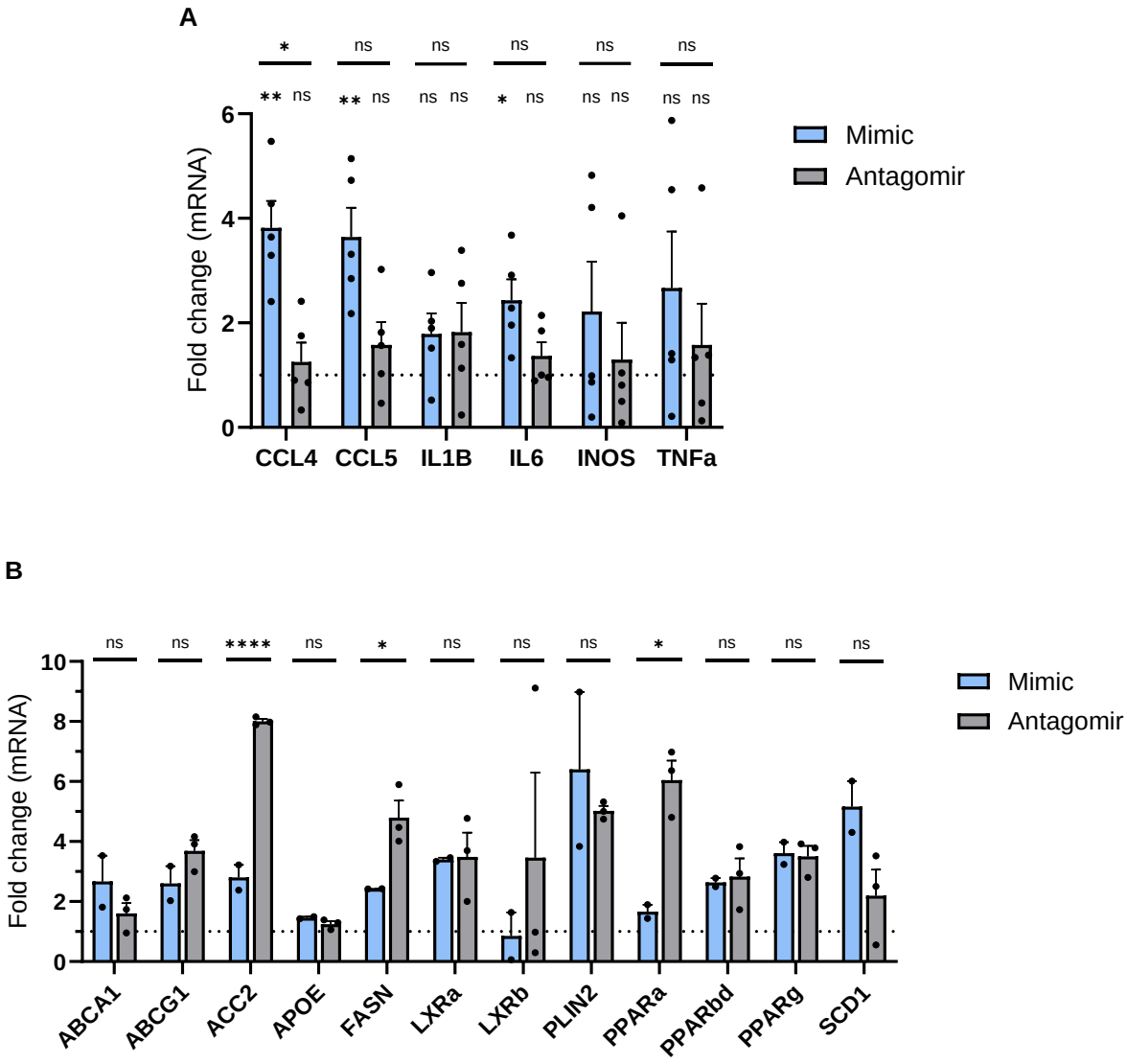

Fig. 5: miR146A overexpression skews macrophages towards an inflammatory phenotype – (**A**) mRNA expression of inflammatory mediators in myelin-treated (100 µg/mL, 24h) WT BMDMs (*n* = 5 wells) transfected with miR-146A mimic (2.5 nM), inhibitor (antagomir, 100 nM), or negative control (scramble) exposed to LPS and IFNg (100 ng/mL, 6h). (**B**) mRNA expression of lipid metabolism genes in myelin-treated WT BMDMs (*n* = 3 wells) transfected with miR-146A mimic, inhibitor (antagomir), or negative control (scramble). Data is represented as mean ± SEM. (*, P < 0.05; **, P < 0.01; ****, P < 0.0001). The dotted lines represent myelin-treated cells exposed to scramble.

DISCUSSION

Multiple sclerosis (MS) is a complex autoimmune disease characterized by inflammation, demyelination, and neurodegeneration. In this study, we investigated the role of miRNAs in MS pathogenesis, focusing on their impacts on myelin debris clearance and inflammatory response in macrophages. Of particular interest is miR-146A, which negatively regulates the NF-κB signaling pathway, the key mediator of inflammation (24). Experimental studies have shown that miR-146A mimics can enhance remyelination in a cuprizone mouse model (25).

Our findings reveal significant alterations in miR-146A expression levels in human MS lesions and myelin-treated phagocytes, as opposed to their respective controls. The observed upregulation of miR-146A suggests its involvement in modulating inflammatory responses associated with MS. This finding is consistent with previous studies indicating the regulatory role of miR-146A in inflammation and its therapeutic significance in atherosclerosis (20).

We present evidence that miR-146A negatively impacts lipid metabolism, demonstrated by the increased lipid droplet accumulation in myelin-treated macrophages transfected with a miR-146A mimic. Likewise, inhibiting miR-146A with antagomir significantly reduces lipid droplet accumulation and even more so upon prolonged myelin exposure. Despite that miR-146A enhances phagocytotic activity in endotoxin-stimulated macrophages by (26) our investigation into phagocytosis revealed no differences in myelin uptake among macrophages with different miR-146A modulation. This suggests that the increased lipid load observed in miR-146A mimic-treated macrophages does not directly result from an enhanced phagocytic activity. Yet, to our surprise, we observed no significant difference in efflux, nor the expression of cholesterol transporters *Abca1* and *Abcg1* between mimic and antagomir-treated BMDMs, suggesting that another compensatory mechanism is involved in regulating the intracellular phagocytic lipid load.

The protective effects of miR-146A inhibition on lipid load in BMDMs can partly be explained by an increase in fatty acid oxidation, through the upregulation of *Pparα (*23*)*. Contradictory, from the increased expression of key lipogenic genes *Acc2* and *Fasn* upon antagomir transfection, we would expect a subsequent decrease and increase in fatty-acid oxidation and synthesis, respectively (21). The resulting switch to a lipid-storing state, in turn, would increase the lipid overload. Hence, the observation that miR-146 inhibition leads to increased expression of fatty acid synthesis genes is paradoxical with the decreased lipid load in antagomir-transfected BMDMs, emphasizing the complex regulatory mechanisms through which miR-146A operates.

Furthermore, our results demonstrate transfection of BMDMs with miR-146A mimics skews macrophages towards a pro-inflammatory phenotype, despite repressing NF-κB and TLR4 signaling pathways (24,27). A possible explanation could be that other regulators of inflammations, such as miR-155 compensate for alterations in miR-146A levels. Accordingly, studies show that miR-155 is overexpressed in miR-146A-deficient mice upon LPS exposure, with an increase in inflammatory mediators (28). Moreover, double deficiency in both miR-146A and miR-155 decreases inflammation upon LPS stimulation (28). Considering this, we postulate that miR-146A, along with other miRNAs such as miR-155, is involved in the fine-tuning of inflammatory responses. Nonetheless, future studies are warranted to elucidate an association between miR-155 and miR-146A in their role in inflammation or myelin debris metabolism.

Challenges – One challenge that is common to miRNA therapeutics in practically all disease contexts is the potential for undesirable off-target effects (29). MiRNAs, including those described above, typically have hundreds of target genes (30), therefore significantly modifying the activity of even a single miRNA can result in the expression of several genes that are unrelated to the desired therapeutic effect. Therefore, future research on the adverse side effects of targeting miR-146A is advised.

A limitation of this study is the lack of assessment regarding sex-specific impact since only female mice were utilized. However, this limitation can be deemed less significant given the higher prevalence of MS in females compared to males.

Future perspectives – Considering that miR-146A affects lipid accumulation and inflammation, future studies could investigate whether the positive impact of targeting miR-146A extends to remyelination. Additionally, miR-146A could be useful as a diagnostic tool to estimate the MS disease severity, although more clinical research is necessary to do so.

In summary, our research has demonstrated that miR-146A is a highly promising therapeutic target for mitigating myelin-induced lipid overload. Furthermore, this approach supports the development of a phagocytic environment that is anti-inflammatory, which is essential for the effective clearance of myelin debris and the resolution of inflammation.

CONCLUSION

Although MS has a multi-faceted disease progression, defective myelin debris metabolism remains a major cause. While further investigations into the *in vivo* potential of miRNAs in MS are warranted to elucidate their potential as a therapy fully, these findings confirm that the impact of miR-146A on lipid overload represents a promising avenue for further research. Targeting this pathway can enhance lipid metabolism and promote a pro-regenerative phagocytic phenotype within the CNS, offering therapy for progressive MS patients and potentially others with demyelinating pathologies.

REFERENCES

1. Bogie, J. F. J., Grajchen, E., Wouters, E., Corrales, A. G., Dierckx, T., Vanherle, S., Mailleux, J., Gervois, P., Wolfs, E., Dehairs, J., Van Broeckhoven, J., Bowman, A. P., Lambrichts, I., Gustafsson, J., Remaley, A. T., Mulder, M., Swinnen, J. V., Haidar, M., Ellis, S. R., Ntambi, J. M., Zelcer, N., and Hendriks, J. J. A. (2020) Stearoyl-CoA desaturase-1 impairs the reparative properties of macrophages and microglia in the brain. *J Exp Med* **217**
2. Cantuti-Castelvetri, L., Fitzner, D., Bosch-Queralt, M., Weil, M. T., Su, M., Sen, P., Ruhwedel, T., Mitkovski, M., Trendelenburg, G., Lütjohann, D., Möbius, W., and Simons, M. (2018) Defective cholesterol clearance limits remyelination in the aged central nervous system. *Science* **359**, 684-688
3. Bogie, J. F., Stinissen, P., and Hendriks, J. J. (2014) Macrophage subsets and microglia in multiple sclerosis. *Acta Neuropathol* **128**, 191-213
4. Grajchen, E., Hendriks, J. J. A., and Bogie, J. F. J. (2018) The physiology of foamy phagocytes in multiple sclerosis. *Acta Neuropathol Commun* **6**, 124
5. Miron, V. E., Boyd, A., Zhao, J. W., Yuen, T. J., Ruckh, J. M., Shadrach, J. L., van Wijngaarden, P., Wagers, A. J., Williams, A., Franklin, R. J. M., and Ffrench-Constant, C. (2013) M2 microglia and macrophages drive oligodendrocyte differentiation during CNS remyelination. *Nat Neurosci* **16**, 1211-1218
6. Kotter, M. R., Li, W.-W., Zhao, C., and Franklin, R. J. M. (2006) Myelin Impairs CNS Remyelination by Inhibiting Oligodendrocyte Precursor Cell Differentiation. *The Journal of Neuroscience* **26**, 328-332
7. Esau, C., Davis, S., Murray, S. F., Yu, X. X., Pandey, S. K., Pear, M., Watts, L., Booten, S. L., Graham, M., McKay, R., Subramaniam, A., Propp, S., Lollo, B. A., Freier, S., Bennett, C. F., Bhanot, S., and Monia, B. P. (2006) miR-122 regulation of lipid metabolism revealed by in vivo antisense targeting. *Cell Metab* **3**, 87-98
8. Raitoharju, E., Lyytikäinen, L.-P., Levula, M., Oksala, N., Mennander, A., Tarkka, M., Klopp, N., Illig, T., Kähönen, M., Karhunen, P. J., Laaksonen, R., and Lehtimäki, T. (2011) miR-21, miR-210, miR-34a, and miR-146a/b are up-regulated in human atherosclerotic plaques in the Tampere Vascular Study. *Atherosclerosis* **219**, 211-217
9. Djuranovic, S., Nahvi, A., and Green, R. (2012) miRNA-mediated gene silencing by translational repression followed by mRNA deadenylation and decay. *Science* **336**, 237-240

10. Thamilarasan, M., Koczan, D., Hecker, M., Paap, B., and Zettl, U. K. (2012) MicroRNAs in multiple sclerosis and experimental autoimmune encephalomyelitis. *Autoimmunity Reviews* **11**, 174-179
11. Junker, A., Krumbholz, M., Eisele, S., Mohan, H., Augstein, F., Bittner, R., Lassmann, H., Wekerle, H., Hohlfeld, R., and Meinl, E. (2009) MicroRNA profiling of multiple sclerosis lesions identifies modulators of the regulatory protein CD47. *Brain* **132**, 3342-3352
12. Vanherle, S., Jorissen, W., Dierckx, T., Loix, M., Grajchen, E., Mingneau, F., Guns, J., Gervois, P., Lambrichts, I., Dehairs, J., Swinnen, J. V., Mulder, M. T., Remaley, A. T., Haidar, M., Hendriks, J. J. A., and Bogie, J. J. F. (2022) The ApoA-I mimetic peptide 5A enhances remyelination by promoting clearance and degradation of myelin debris. *Cell Reports* **41**
13. Li, K., Zhao, B., Wei, D., Wang, W., Cui, Y., Qian, L., and Liu, G. (2020) miR-146a improves hepatic lipid and glucose metabolism by targeting MED1. *Int J Mol Med* **45**, 543-555
14. Marschallinger, J., Iram, T., Zardeneta, M., Lee, S. E., Lehallier, B., Haney, M. S., Pluvinage, J. V., Mathur, V., Hahn, O., Morgens, D. W., Kim, J., Tevini, J., Felder, T. K., Wolinski, H., Bertozzi, C. R., Bassik, M. C., Aigner, L., and Wyss-Coray, T. (2020) Lipid-droplet-accumulating microglia represent a dysfunctional and proinflammatory state in the aging brain. *Nature Neuroscience* **23**, 194-208
15. Bogie, J. F. J., Haidar, M., Kooij, G., and Hendriks, J. J. A. (2020) Fatty acid metabolism in the progression and resolution of CNS disorders. *Adv Drug Deliv Rev* **159**, 198-213
16. Ouimet, M., Franklin, V., Mak, E., Liao, X., Tabas, I., and Marcel, Y. L. (2011) Autophagy regulates cholesterol efflux from macrophage foam cells via lysosomal acid lipase. *Cell Metab* **13**, 655-667
17. Vazquez, M. M., Gutierrez, M. V., Salvatore, S. R., Puiatti, M., Dato, V. A., Chiabrando, G. A., Freeman, B. A., Schopfer, F. J., and Bonacci, G. (2020) Nitro-oleic acid, a ligand of CD36, reduces cholesterol accumulation by modulating oxidized-LDL uptake and cholesterol efflux in RAW264.7 macrophages. *Redox Biol* **36**, 101591
18. Cantuti-Castelvetri, L., Fitzner, D., Bosch-Queralt, M., Weil, M.-T., Su, M., Sen, P., Ruhwedel, T., Mitkovski, M., Trendelenburg, G., Lütjohann, D., Möbius, W., and Simons, M. (2018) Defective cholesterol clearance limits remyelination in the aged central nervous system. *Science* **359**, 684-688
19. Li, K., Ching, D., Luk, F. S., and Raffai, R. L. (2015) Apolipoprotein E Enhances MicroRNA-146a in Monocytes and Macrophages to Suppress Nuclear Factor-κB–Driven Inflammation and Atherosclerosis. *Circulation Research* **117**, e1-e11
20. Fish, J. E., and Cybulsky, M. I. (2015) ApoE Attenuates Atherosclerosis via miR-146a. *Circulation Research* **117**, 3-6
21. Saha, A. K., and Ruderman, N. B. (2003) Malonyl-CoA and AMP-activated protein kinase: an expanding partnership. *Mol Cell Biochem* **253**, 65-70
22. Gonzalez-Bohorquez, D., Gallego López, I. M., Jaeger, B. N., Pfammatter, S., Bowers, M., Semenkovich, C. F., and Jessberger, S. (2022) FASN-dependent de novo lipogenesis is required for brain development. *Proceedings of the National Academy of Sciences* **119**, e2112040119
23. Xu, J., Xiao, G., Trujillo, C., Chang, V., Blanco, L., Joseph, S. B., Bassilian, S., Saad, M. F., Tontonoz, P., Lee, W. N. P., and Kurland, I. J. (2002) Peroxisome Proliferator-activated Receptor α (PPARα) Influences Substrate Utilization for Hepatic Glucose Production*. *Journal of Biological Chemistry* **277**, 50237-50244
24. Taganov, K. D., Boldin, M. P., Chang, K. J., and Baltimore, D. (2006) NF-kappaB-dependent induction of microRNA miR-146, an inhibitor targeted to signaling proteins of innate immune responses. *Proc Natl Acad Sci U S A* **103**, 12481-12486
25. Zhang, J., Zhang, Z. G., Lu, M., Wang, X., Shang, X., Elias, S. B., and Chopp, M. (2017) MiR-146a promotes remyelination in a cuprizone model of demyelinating injury. *Neuroscience* **348**, 252-263

26. Cao, Z., Yao, Q., and Zhang, S. (2015) MiR-146a activates WAVE2 expression and enhances phagocytosis in lipopolysaccharide-stimulated RAW264.7 macrophages. *Am J Transl Res* **7**, 1467-1474
27. Boldin, M. P., Taganov, K. D., Rao, D. S., Yang, L., Zhao, J. L., Kalwani, M., Garcia-Flores, Y., Luong, M., Devrekanli, A., Xu, J., Sun, G., Tay, J., Linsley, P. S., and Baltimore, D. (2011) miR-146a is a significant brake on autoimmunity, myeloproliferation, and cancer in mice. *Journal of Experimental Medicine* **208**, 1189-1201
28. Mann, M., Mehta, A., Zhao, J. L., Lee, K., Marinov, G. K., Garcia-Flores, Y., Lu, L. F., Rudensky, A. Y., and Baltimore, D. (2017) An NF-κB-microRNA regulatory network tunes macrophage inflammatory responses. *Nat Commun* **8**, 851
29. Winkle, M., El-Daly, S. M., Fabbri, M., and Calin, G. A. (2021) Noncoding RNA therapeutics - challenges and potential solutions. *Nat Rev Drug Discov* **20**, 629-651
30. Friedman, R. C., Farh, K. K., Burge, C. B., and Bartel, D. P. (2009) Most mammalian mRNAs are conserved targets of microRNAs. *Genome Res* **19**, 92-105

Acknowledgements – The work was financially supported by the Research Foundation of Flanders (FWO Vlaanderen). The funding agencies had no role in the design, analysis, or writing of the manuscript. Prof. J. Bogie is gratefully acknowledged for providing his expertise in the domain. S. Vanherle and B. Moonen are gratefully acknowledged for their excellent technical assistance. K. Kuipers is thanked for providing access to his ORO script in ImageJ.

Author contributions – SV and JB conceived and designed the research. SV and DK performed experiments and data analysis. SV and DK wrote the paper. SV, BM, and JG assisted in several experiments. All authors carefully edited the manuscript

SUPPLEMENTAL INFORMATION

Table 1S – Primer sequences used for qPCR amplification.

Gene	Forward (5'–3')	Reverse (5'–3')	Accession Number
Cyca	AGACTGAGTGGTTGGATGGC	TCGAGTTGTCCACAGTCAGC	NM_009828
Tbp	CTACCGTGAATCTTGGCTGTAAAC	AATCAACGCAGTTGTCCGTGGC	NM_013684
U6	GCTTCGGCAGCACATATACTAAAAT	CGCTTCACGAATTTGCGTGTCAT	X59362
Rnu5g	AAAGATTTCCGTGGAGAGGAACAA	TTGAGCCTTGCTCCGACAAGGCTA	NR_002852
miR-146A	TGAGAACTGAATTCCATGGG	GAACATGTCTGCGTATCTC	MI0000919
miR-155	AATGCTAATTGTGATAGGGG	GAACATGTCTGCGTATCTC	MI0000177
Ccl4	ACCCTCCCACTTCCTGCTGTTT	CTGTCTGCCTCTTTTGGTCAGG	NM_013652
Ccl5	CCTGCTGCTTTGCCTACCTCTC	ACACACTTGGCGGTTCCTTCGA	NM_013653
Il1b	TGGACCTTCCAGGATGAGGACA	GTTCATCTCGGAGCCTGTAGTG	NM_008361
Il6	TACCACTTCACAAGTCGGAGGC	CTGCAAGTGCATCATCGTTGTTC	NM_031168
Inos	GAGACAGGGAAGTCTGAAGCAC	CCAGCAGTAGTTGCTCCTCTTC	NM_010927
Tnfα	GGTGCCTATGTCTCAGCCTCTT	GCCATAGAACTGATGAGAGGGAG	NM_013693
Abca1	GGAGCCTTTGTGGAACTCTTCC	CGCTCTCTTCAGCCACTTTGAG	NM_013454
Abcg1	GACACCGATGTGAACCCGTTTC	GCATGATGCTGAGGAAGGTCCT	NM_009593
Acc2	TGCTGACAGAGGCACCACTGAA	CAGTTGTACGTCCAGAGGCATAG	NM_007392
ApoE	GAACCGCTTCTGGGATTACCTG	GCCTTTACTTCCGTCATAGTGTC	NM_009696
Fasn	CACAGTGCTCAAAGGACATGCC	CACCAGGTGTAGTGCCTTCCTC	NM_007988
Lxrα	TGTTGCAGCCTCTCTACTTGGA	TCTGCAGACCGGCCCAACGTG	NM_013839
Lxrb	AAGGACTTCACCTACAGCAAGGA	GAACTCGAAGATGGGATTGATGA	NM_009473
Plin2	GACAGGATGGAGGAAAGACTGC	GGTAGTCGTCACCACATCCTTC	NM_007408
Pparα	ACCACTACGGAGTTCACGCATG	GAATCTTGCAGCTCCGATCACAC	NM_011144
Pparb/d	GGACCAGAACACACGCTTCCTT	CCGACATTCCATGTTGAGGCTG	NM_011145
Pparg	GTACTGTCGGTTTCAGAAGTGCC	ATCTCCGCCAACAGCTTCTCCT	NM_011146
Scd1	GCAAGCTCTACACCTGCCTCTT	CGTGCCTTGTAAGTTCTGTGGC	NM_009127

An overview of the forward and reverse primer sequences of mouse target genes and their respective accession numbers, as used in qPCR.